Industrial Crops & Products 129 (2019) 15–23

Contents lists available at ScienceDirect

Industrial Crops & Products

journal homepage: www.elsevier.com/locate/indcrop

Lignin containing cellulose nanofibril production from willow bark at 80 °C using a highly recyclable acid hydrotrope

Jinze Dou[a], Huiyang Bian[b], Daniel J. Yelle[b], Mariko Ago[a], Krista Vajanto[c], Tapani Vuorinen[a,*], Junyong (J.Y.) Zhu[b,*]

[a] Department of Bioproducts and Biosystems, School of Chemical Engineering, Aalto University, P.O. Box 16300, 00076, Espoo, Finland
[b] USDA Forest Service, Forest Products Laboratory, Madison, WI, USA
[c] Department of Applied Physics, School of Science, Aalto University, P.O. Box 11100, 00076 Espoo, Finland

ARTICLE INFO

Keywords:
Nanocellulose
Suberin
Aromatic substance
5-Hydroxymethylfurfural
p-Toluenesulfonic acid
Willow bark

ABSTRACT

We conducted the first comparative exploration on lignin containing cellulose nanofibril films prepared alternatively from willow bark and wood using a highly recyclable acid hydrotrope, aqueous *p*-toluenesulfonic acid, as a sustainable means for isolating the nanofibrils. The nanofibrils of willow bark were hydrophobic and produced dense films of high strength under hot pressing. The hydrophobicity resulted from condensation of the residual lignin with low molecular weight aromatic substances of the bark and hydroxymethylfurfural formed *in situ* from fructose that is also present in the bark.

1. Introduction

Lignocelluloses being a renewable resource have attracted great interests in many fields. The key to successful and sustainable lignocellulose based economic growth is developing green processing technologies to produce basic building blocks such as cellulose nanofibrils and nanocrystals for a variety of applications (Rajala et al., 2016; Zhu et al., 2016; Giese et al., 2015).

Existing technologies for producing cellulose nanofibrils (CNF) or cellulose nanocrystals (CNC) include hydrolysis with mineral acids, such as phosphoric and sulfuric acid (Espinosa et al., 2013; Chen et al., 2015), or dicarboxylic acids (Chen et al., 2016; Wang et al., 2017; Qin et al., 2016), as well as catalytic oxidation with hypochlorite (Pääkkönen et al., 2016; Saito and Isogai, 2004). Unfortunately, economic recovery of mineral acids or the oxidation catalysts is difficult. Although, using concentrated solid dicarboxylic acid hydrolysis for producing cellulose nanomaterials (Chen et al., 2016; Wang et al., 2017) addressed the issue of acid recovery, the existing processes require chemical pulp or cotton as the raw material. Manufacture of cellulose nanomaterials directly from low cost biomass fractions would be desirable but very difficult to achieve due to the rigid, recalcitrant structure of the plant cell wall. Although direct mechanical fibrillation of lignified biomass to nanofibrils consumes large amounts of electricity (Hoeger et al., 2013), simple chemical pretreatments can facilitate the mechanical fibrillation and lower the need of energy. Recently, *p*-toluenesulfonic acid (*p*-TsOH), a commercial catalyst, was found to have hydrotropic properties and capability of rapidly solubilizing wood lignin in aqueous solutions at low temperatures (< 100 °C) (Bian et al., 2017; Chen et al., 2017). The approach can be used to produce lignin containing cellulose nanomaterials with hydrophobic properties. As a solid catalyst, *p*-TsOH can be relatively easily recycled and it can catalyze the dehydration of solubilized hemicellulosic sugars into furans as valuable chemicals. Furthermore, the solubilized lignin can be recovered as lignin nanoparticles (LNP) that form a valuable building block for a variety of applications, e.g. bio-based drug delivery vehicles and stabilizers (Frangville et al., 2012).

The objective of this study is to demonstrate that agricultural material from willow bark (WB) and wood (WW) can be used to produce lignin containing cellulose nanofibrils (LCNF) directly by *p*-TsOH fractionation. Willow (*Salix* sp.) plantations have been considered as a sustainable resource for energy production for decades (Krzyżaniak et al., 2015). Previous studies revealed that the high quality sclerenchyma fibres and aromatic extracts from the bark could produce higher value products than fuel (Dou et al., 2016, 2018a). The significance of this study is to further explore the high value utility of willow bark and wood through producing cellulose nanomaterials. Furthermore, the study analyzes the unique nearly native properties of the lignin dissolved by aqueous *p*-TsOH at mild conditions.

* Corresponding authors.
E-mail addresses: tapani.vuorinen@aalto.fi (T. Vuorinen), jzhu@fs.fed.us (J.J. Zhu).

https://doi.org/10.1016/j.indcrop.2018.11.033
Received 18 July 2018; Accepted 13 November 2018
Available online 03 December 2018

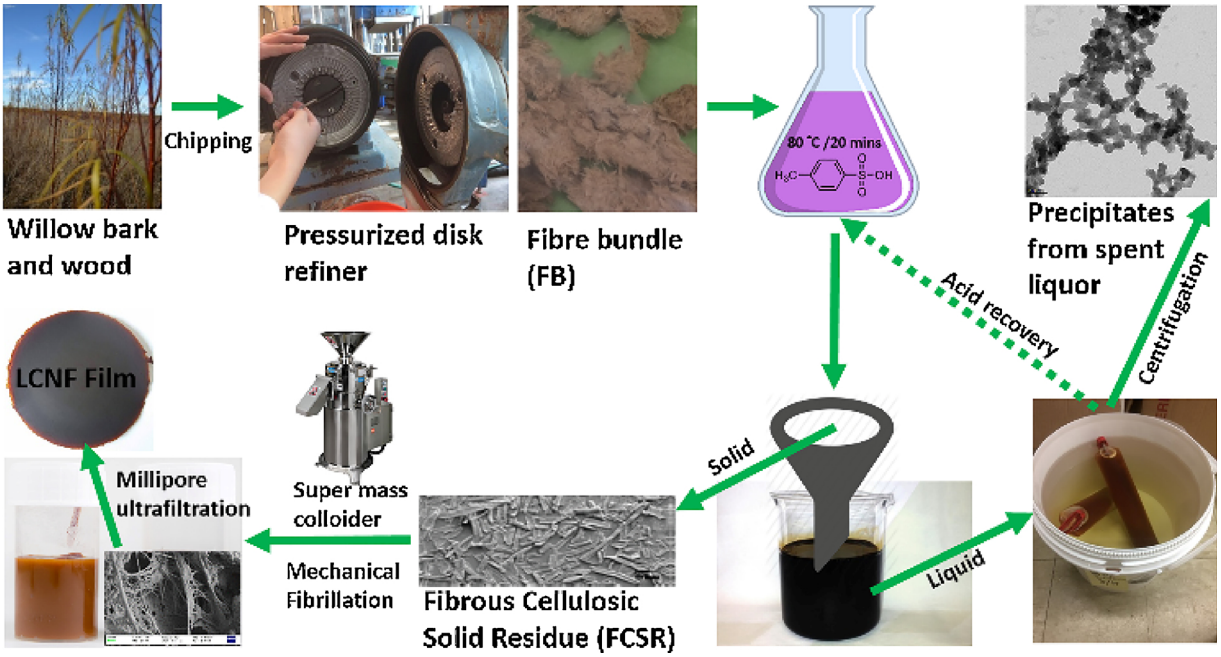

Fig. 1. Experimental flow of fractionation of willow bark and wood for producing LCNF, LCNF film and dissolved lignin using *p*-TsOH. Flows with dashed lines were not implemented in this study.

Table 1
Glycan and lignin contents (%) of original, unextracted willow wood, willow bark and the solid fractions obtained from them after treating with aqueous *p*-TsOH for 20 min at 80 °C. The yield of each solid fraction was determined both gravimetrically and from the glucan content assuming that the glucan yield was 100%.

Biomass fraction *p*-TsOH (%)	Wood –	Wood 60	Wood 80	Bark –	Bark 60	Bark 80
Glucose	45.1	57.2	51.4	24.2	31.6	31.5
Xylose	19.2	14.1	8.9	2.7	3.5	1.7
Mannose	2.3	2.8	2.5	1.1	1.7	1.6
Galactose	1.0	0.6	0.4	2.8	1.3	0.6
Arabinose	0.6	0.1	0.1	4.3	0.1	0.2
Rhamnose	0.5	0.3	0.3	0.9	0.3	0.0
Klason lignin	26.8	23.0	22.5	37.3	43.0	42.0
Gravimetric yield	100	60.4	85.4	100	76.6	75.0
Calculated yield	–	78.8	87.7	–	76.6	76.8

2. Material and methods

2.1. Material

All chemicals and solvents used in this study were purchased from VWR and used as supplied. Four-year-old stems of willow hybrid 'Karin' were collected from the plantation at the VTT Technical Research Centre of Finland Ltd. located in Central Finland (Kyyjärvi) on May 13, 2015. The whole stems were stored at −20 °C until use. For separation of bark, the frozen stems were immersed in water at 20 °C overnight before debarking. The bark and wood were manually separated with scalpel and stored at 20 °C until use.

2.2. LCNF and its film preparation

As depicted in Fig. 1, willow bark and wood were first refined in a 30.5 cm pressurized disk refiner (Sprout-Bauer, model 1210P, Muncy, PA, USA) using disk plate pattern of D2B505 with a disk gap of 0.178 mm. The refining feed rate and energy input were respectively ca. 1 kg min^{-1} and 152 Wh/kg, both expressed relative to the oven dry weight (OD). The resultant particles (25 g) were then treated with aqueous *p*-TsOH (60 or 80 wt%) at 80 °C with a liquid-to-biomass (OD) ratio of 10:1. The fibre suspension was constantly mixed using a mixer at 300 rpm. After 20 min the spent liquor was separated by vacuum filtration through a filter paper. The filtered solid was washed using distilled water and collected as a WIS fraction for LCNF production using a super mass colloider (SMC), as visualized at Figure S1. The filtrate was collected for the recovery of acid and dissolved lignin.

The spent acid liquor was diluted using distilled water to approximately 10 wt% acid concentration that is below the minimal *p*-TsOH hydrotrope concentration (Chen et al., 2017). Precipitation of the dissolved lignin was observed. The diluted spent liquor was centrifuged at 10,000 rpm for 10 min (Sorvall Superspeed RC2-B, GSA rotator, Ivan Sorvall, Inc., Norwalk, CT) to separate the precipitated lignin from the excess acid. The lignin obtained was then freeze-dried for ca. 72 h for the NMR analysis.

LCNF suspensions of 1% was screened using a Sefar Nitex polyamine monofilament (pore size of the mesh fabric: 10 μm) under 2.5 bar. The films were pressed for 4 min before further pressed in a Carver Laboratory press (Fred S. Carver Inc.) under 100 °C and at the pressure of 1.8 kPa for 2 h (Österberg et al., 2013).

2.3. Chemical analyses

The carbohydrate and lignin contents of the original willow and the fractionated WIS FCSR were determined. Acetone extraction (NREL/TP-510-42618) was applied to the original willow before the acid hydrolysis. The carbohydrate analyses were performed using ion chromatography through HPAEC-PAD detection (Dionex ICS-3000, Sunnyvale, CA, USA) with CarboPac PA20 column. Pure water was employed as the mobile phase and the elutions were implemented under room temperature at a flow rate of 0.38 mL min^{-1}.

The molar mass distribution of the LCNF sample was characterized by gel permeation chromatography (GPC) to examine the degree of cellulose degradation. The LCNF was first pre-activated in a water/acetone solvent by *N,N*-dimethylacetamide (DMAc) before dissolved in 90 g L^{-1} lithium chloride (LiCl)/ DMAc solvent mixture at room temperature and filtered through a 0.2 mm syringe filter and analyzed by a Dionex Ultimate 3000 system with refractive index (RI) detection

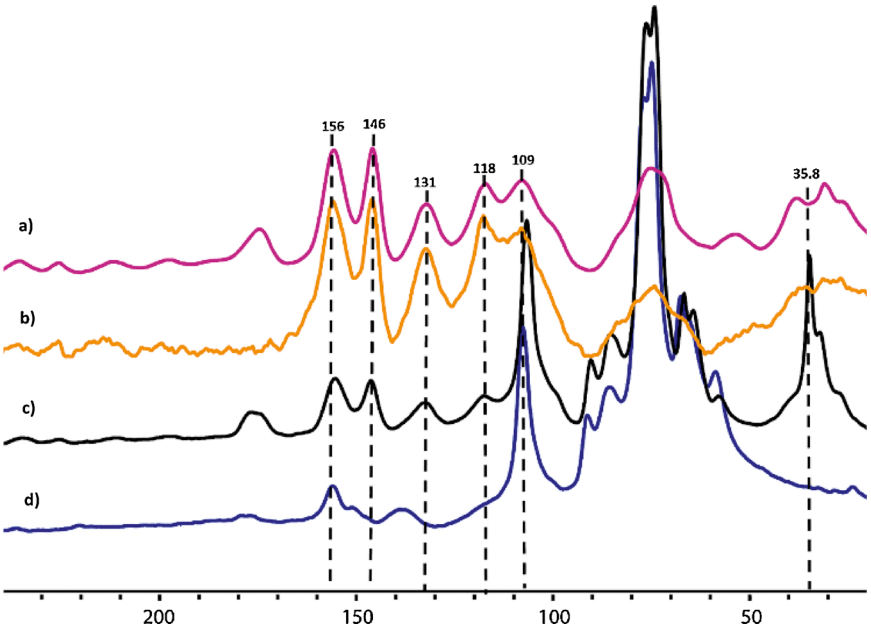

Fig. 2. ^{13}C CP/MAS NMR spectra of: a) Dissolved lignin from treatment of willow bark with 60% *p*-TsOH; b) Precipitate from treatment of hot water extract of willow inner bark with sulfuric acid (Dou et al., 2018a); c) Solid residue from treatment of willow bark with 60% *p*-TsOH; d) Solid residue from treatment of willow wood with 60% *p*-TsOH.

(Shodex RI-101). The intrinsic viscosities of the LCNFs were also determined by following the standard method SCAN-CM 15:99 using cupriethylenediamine (CED) as the solvent.

Solution-state Nuclear Magnetic Resonance (NMR) spectra were acquired on a Bruker BioSpin (Billerica, MA, USA) AVANCE 700 MHz instrument provided with a cryogenically cooled 5 mm QCI $^{1}H/^{31}P/^{13}C/^{15}N$ cryoprobe. Phase-sensitive 2D ^{1}H–^{13}C HSQC spectra (hsqcetgpsisp.2 pulse sequence from the Bruker Library; phase-sensitive gradient-edited 2D HSQC using adiabatic pulses for inversion and refocusing) were acquired with spectral widths of 12 ppm for ^{1}H (1682 data points, and an F2 acquisition time of 100 ms) and 220 ppm for ^{13}C with 620 increments (F1 acquisition time of 8 ms) using 800 scans with a 500 ms interscan delay. The central DMSO/Pyridine solvent peak was taken as an internal reference (δC 39.5, δH 2.49 ppm). (Kim and Ralph, 2010) The processing parameter used typical matched Gaussian apodization and squared cosine-bell apodization in the ^{1}H and ^{13}C dimension, respectively. The volume integration of contours used Bruker's Topspin 3.2 software (Bruker). Image contours were colorized using Adobe Illustrator.

The solid-state ^{13}C CP/MAS spectra of LCNF and dissolved lignin samples (packed inside a 4.0 mm ZrO_2 rotor) were gained on a Bruker AVANCE III spectrometer operating at 100.61 MHz. The following parameters were applied: a spectral width of 306 ppm, a relaxation delay of 5 s, 40 K transients of 2 K data points, a contact time of 1 ms, and a spinning rate of 8 kHz.

2.4. Morphological and physical analyses

Transmission electron microscopy (TEM) grids (Cu grids with continuous carbon films) were plasma cleaned on a Gatan Solarus (Model 950) plasma cleaner for making the grid surface hydrophilic. A drop of 5 µL LCNF or dissolved lignin suspension was placed on the Cu grids followed by removing of water after the drop using filter paper. A drop of 5 µL 1% Uranyl Acetate solution was titrated on the grid for 1 min as a negative stain followed by removing of liquid with filter paper. Thereafter, the grids were examined using the TEM (FEI Tecnai 12) under an accelerating voltage of 120 kV and images were processed using Gatan Digital Micrograph. Scanning electron microscopy (SEM) imaging was performed using a Zeiss Sigma VP. The conductivity of LCNF samples were sputter-coated using gold. The images were taken at 1.7 kV operating voltage.

LCNF fibril dimensions and the fibril morphology were characterized using atomtic force microscopy (AFM) on a NanoScope V multimode scanning microscope (Digital Instruments Inc., Santa Barbara, CA) operating in tapping mode. The driving frequency of the AFM silicon cantilever (NSC15/AIBS, MicroMasch, Tallinn Estonia) was 272.45 kHz. The radius of curvature from the tip was less than 10 nm.

Thermogravimetric analyses (TGA) of the LCNF and the original bark, wood were conducted using a TA Instruments Q 500 (New Castle, DE) with a temperature program at a heating rate of 10 °C min^{-1} from ambient temperature to 600 °C. Approximately 5 mg of sample was used for each test. A flow rate of 40 mL min^{-1} nitrogen source was opened into the furnace for preventing any oxidative decomposition.

The water contact angle on the films was characterized using a CAM 200 (KSV Instruments Ltd., Helsinki, Finland). The pure water drop volume and the rate were 7 µL and 1 µL/s, respectively.

Dynamic Vapor Sorption (DVS) apparatus (Surface Measurement system, London, UK) at the measuring accuracy up to 0.1 µg was used for water vapor analysis of LCNF. Roughly 10 mg LCNF powder was kept at the sample pan at 25 °C at 0% RH under a flow of nitrogen gas (100 cm^3s^{-1}) until the mass equilibrated. The adsorption and desorption cycling followed the method of Ma et al. (Ma et al., 2015)

Density of the LCNF films was computed by dividing sample basis weight (TAPPI standard T410) by the specimen size (15 mm wide and 72 mm long) and its thickness (TAPPI Method T411). Tensile tests were carried out using an MTS 400/M Vertical Tensile Tester equipped with a 200 N load cell at a cross-head speed of 5 mm min^{-1} (ISO 527-2). The tensile strength, tensile index, breaking strain, and elastic modulus were obtained from the stress-strain curves.

3. Results and discussion

3.1. Chemical composition of the solid fraction

In average, the aqueous *p*-TsOH treatments solubilized ca. 17 and 24% of the willow wood and bark, respectively (Table 1). The yield of cellulose and (gluco)mannan was practically quantitative while half of xylan was solubilized. Pectins that are known to be present in the bark were largely removed as indicated by the decrease in the content of the characteristic pectic sugars, arabinose, rhamnose and, in part, galactose. In the case of willow wood, ca. 30% of the lignin, measured as the acid insoluble Klason lignin, was solubilized. ^{13}C CP/MAS NMR

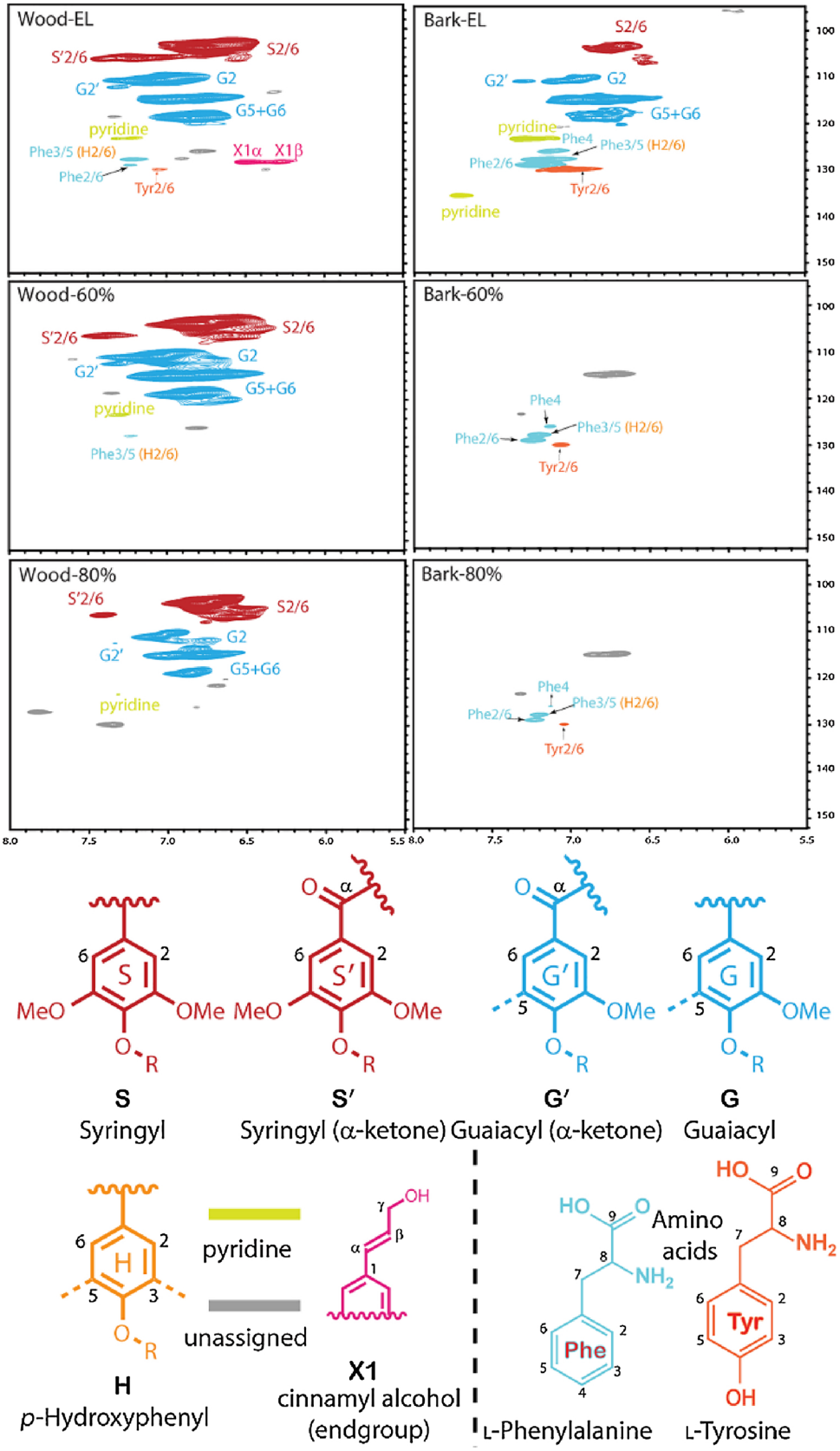

Fig. 3. Aromatic region of HSQC NMR spectra of the materials precipitated from the spent liquor after treating willow wood (WW) and willow bark (WB) in aqueous *p*-TsOH. The spectra of lignins isolated enzymatically (EL) from the wood and bark are also included. (Dou et al., 2018b).

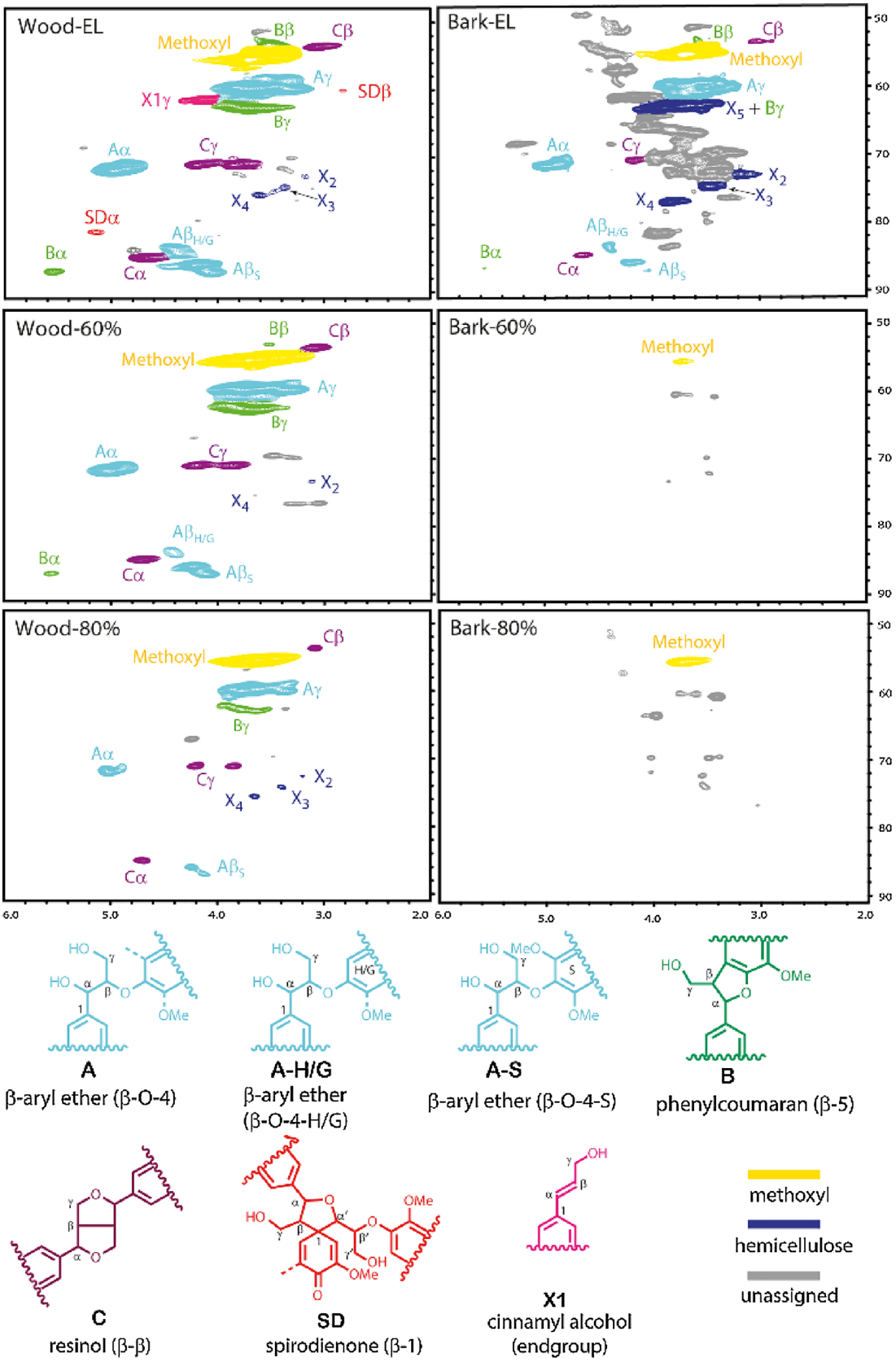

Fig. 4. Side-chain region of HSQC NMR spectra of the materials precipitated from the spent liquor after treating willow wood (WW) and willow bark (WB) in aqueous *p*-TsOH. The spectra of lignins isolated enzymatically (EL) from the wood and bark are also included. (Dou et al., 2018b).

Table 2
Relative abundances of aromatic units and interunit linkages in enzymatically isolated lignins (EL) from willow wood and bark (Dou et al., 2018b) and dissolved lignins precipitated from spent liquors after treating willow wood and bark with 60 or 80 % *p*-TsOH.

Origin *p*-TsOH (%)	Wood EL	Wood 60	Wood 80	Bark EL	Bark 60	Bark 80
Linkage type (%)[a]						
β-*O*-4 (A)	89	72	66	86	64	54
β-5 (B)	3	6	7	2	–	–
β-β (C)	7	21	27	12	36	46
Monomers[b]						
G (%)	34	29	22	61	–	–
S (%)	66	71	78	39	–	–
S/G ratio	1.9	2.5	3.5	0.6	–	–

[a] Percentage on the sum of the α-carbon integrals for structures A, B and C (Aα, Bα, and Cα in Fig. 4).
[b] Expressed as a percentage on total signal intensity of guaiacyl (G2 + G2′) and syringyl units (S2/6 + S′2/6) in each case (Fig. 3).

spectroscopy of the solid residues from willow wood confirmed that they composed mainly of cellulose (C-1 at 109 ppm, C-2 to C-6 in 60–90 ppm region) and syringyl-guaiacyl type of lignin (aromatic signals in 130–160 ppm region, OCH_3 at 58.5 ppm) (Fig. 2d, Figures S2-S3) (Kono et al., 2002; Idström et al., 2016; Sannigrahi et al., 2011). The major cellulose signals and a minor methoxyl signal were also present in the ^{13}C CP/MAS NMR spectra of the solid residues from willow bark (Fig. 2c, Figures S4-S5). The aromatic lignin signals were overlapped with strong ^{13}C NMR signals at 118, 131, 146 and 156 ppm. These signals are characteristic for the condensation products of low molecular weight aromatic compounds and hydroxymethylfurfural which were earlier identified when a hot water extract from willow inner bark was treated under acid conditions (Fig. 2b) (Dou et al., 2018a; van Zandvoort et al., 2013). Here, the condensation took place in the aqueous *p*-TsOH treatment, thus increasing the mass of the acid insoluble Klason lignin fraction. Without the condensation these low molecular weight compounds would have been extracted from the sample prior to the analytical Klason lignin determination. Moreover, the solid residue of willow bark gave rise to additional major ^{13}C NMR signals at 20–45 ppm and 170–180 ppm. These signals were neither present in the solid residue of willow wood nor the condensation products of the inner bark extract (Dou et al., 2018a). Obviously, the narrow methylene signals at ca. 35 ppm originated from suberin (Ferreira et al., 2014) that has been reported to be present in the bark of several trees, e.g. *Platanus orientalis* (Dönmez et al., 2016), *salix* (Trockenbrodt, 1994) and beech (Perra et al., 1993), as well as in specialized plant cell walls (Graça, 2015). In conclusion, the high Klason lignin content of the solid residue of willow bark does not only represent lignin but also a variety of other bark components condensed with it.

Figure S6 and Table S1 summarize the molar mass distributions of the solid residues from willow wood and bark after treating them with aqueous *p*-TsOH. In most cases a bimodal molar mass distribution was observed where the lower molar mass region, in principle, could represent hemicelluloses, lignin and/or depolymerized cellulose. When the differences in the cellulose contents are taken into account, the viscosities of the residues solubilized in aqueous CED were comparable indicating no major difference in depolymerisation of cellulose between wood and bark (Table S2).

3.2. Structure of the dissolved and precipitated material

When the spent liquors from the treatment of willow wood with aqueous *p*-TsOH were diluted with water, precipitates were formed that were then isolated by centrifugation. ^{1}H–^{13}C NMR correlation (HSQC) spectroscopy of solutions of the precipitates provided spectra typical for syringyl-guaiacyl type of lignin (Figs. 3 and 4). The spectral data were assigned and referenced using previously published literature and compared with the NMR data on enzymatically isolated willow wood and bark lignins (Dou et al., 2018b; Kim et al., 2008; Yelle et al., 2008; Kim et al., 2017). Integration of the signal intensities in the aromatic (δ_C/δ_H 95–152/5.5–8.0 ppm) and side-chain (48–91/2.0–6.0 ppm) regions provided information on the relative abundancies of the monomers and interunit linkage types, respectively (Table 2). The lignin dissolved from willow wood was structurally quite similar to the

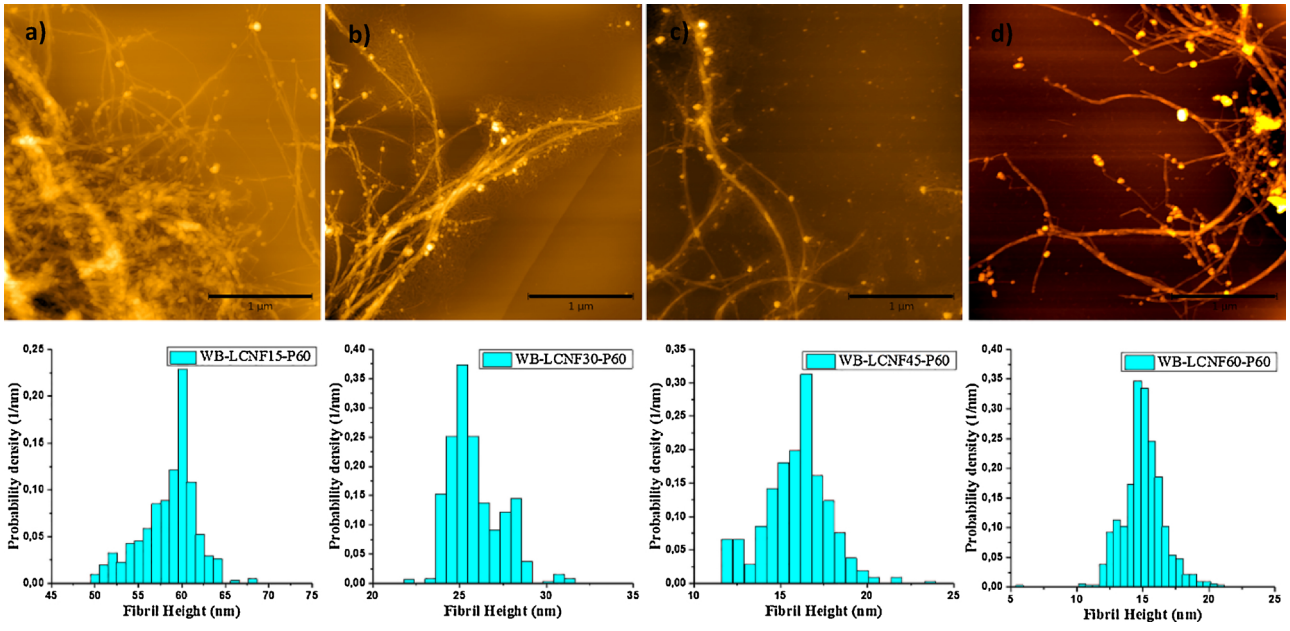

Fig. 5. Effect of SMC milling time on fibrillation of the solid residue of willow bark from the fractionation with 60% *p*-TsOH characterized by AFM images (top), along with LCNF height distributions (bottom): a) 15 min, mean fibril thickness (MFT) = 58.6 nm; b) 30 min, MFT = 25.9 nm; c) 45 min, MFT = 16.0 nm; d) 60 min, MFT = 15.1 nm.

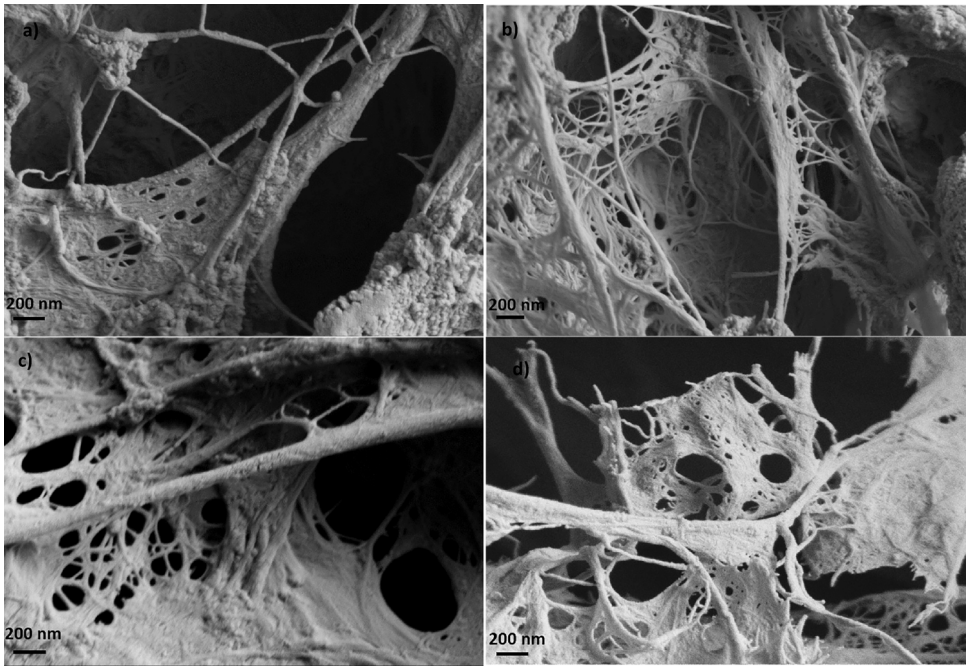

Fig. 6. SEM images of LCNF prepared from the solid residues of willow bark and wood with 60 min SMC milling time. a) Bark, 60% *p*-TsOH; b) Bark, 80% *p*-TsOH; c) Wood, 60% *p*-TsOH; d) Wood, 80% *p*-TsOH.

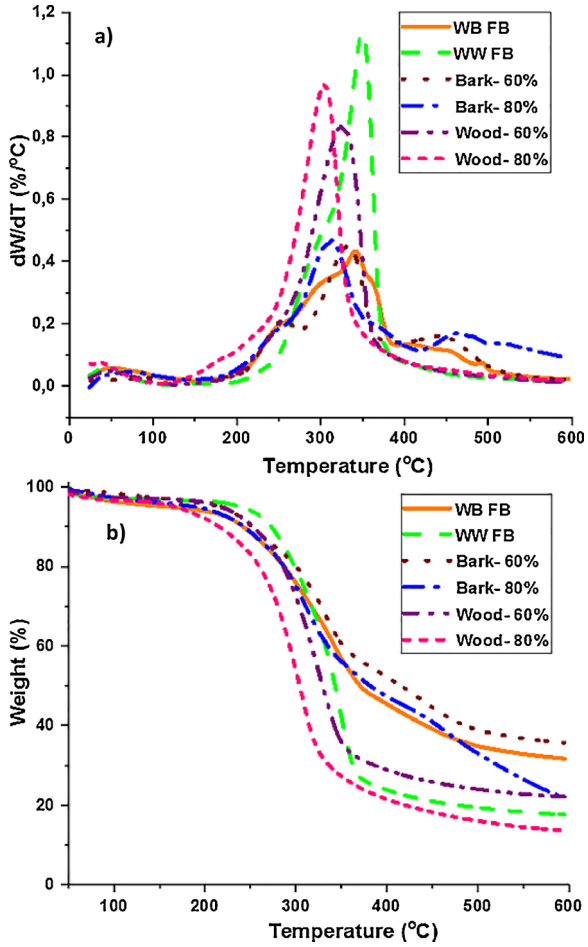

Fig. 7. Weight loss rate (a) and weight gain (b) of willow bark (WB), willow wood (WW) and LCNF made of them after fractionation with 60 or 80% *p*-TsOH. All LCNF were prepared using 60 min SMC milling time.

Table 3
Water contact angle (WCA) of LCNF films produced from willow bark and wood after their treatment with 60 or 80 % *p*-TsOH. All LCNF were prepared using 60 min SMC milling time. The images show the shape of water droplets on the LCNF films.

Origin	Bark	Bark	Wood	Wood
p-TsOH (%)	60	80	60	80
WCA (°)	104 ± 5.0	77 ± 7.2	71 ± 7.7	65 ± 5.3

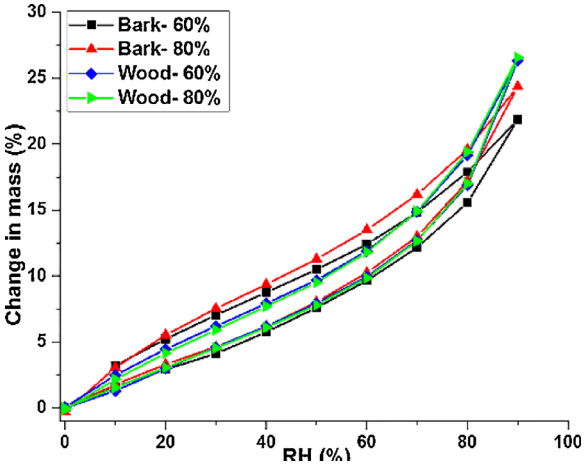

Fig. 8. Moisture sorption/desorption isotherms of LCNF made of willow bark and wood using 60 and 80% aqueous *p*-TsOH. All LCNF were prepared using 60 min SMC milling time.

original lignin even though syringyl units and resinol (β-β) and phenylcoumaran (β-5) structures were more abundant in the dissolved lignin. However, the cinnamyl alcohol end groups ($C_\alpha H$ at 6.54/129.1 and $C_\beta H$ at 6.32/129.0 ppm) seemed to disappear in the *p*-TsOH

Table 4
Density and tensile properties of the LCNF films. The numbers in the parentheses are the standard deviation. ND = not determined.

Origin	Bark	Bark	Wood	Wood
p-TsOH (%)	60	80	60	80
Density (g/cm^3)	1.17 (0.04)	1.17 (0.04)	1.23 (0.05)	1.18 (0.08)
Grammage (g/m^2)	124.7 (5.90)	106.3 (15.75)	98.8 (2.53)	84.9 (3.78)
Tensile strength (MPa)	54.7 (13.22)	29.6 (15.33)	29.1 (ND)	31.9 (16.68)
Tensile index (kNm/kg)	46.8 (11.31)	25.5 (13.19)	23.7 (ND)	27.1 (14.19)
Breaking strain (%)	0.94 (0.21)	0.50 (0.19)	0.46 (ND)	0.48 (0.19)
Elastic modulus (GPa)	6.0 (0.36)	5.6 (1.26)	6.2 (ND)	6.5 (1.54)
Specific elastic modulus (MNm/kg)	5.2 (0.31)	4.9 (1.09)	5.1 (ND)	5.5 (1.31)

treatment. Very strong OCH_3 signals at 58.5 ppm, typical of lignin, were present both in HSQC and ^{13}C CP/MAS NMR spectra of the precipitated dissolved material (Figures S7 and S8).

^{13}C CP/MAS NMR spectroscopy of the substance precipitated from the spent liquor from the treatment of willow bark with aqueous *p*-TsOH showed little similarity with lignin (Fig. 2a). Instead, structures identical with those in the solid condensation product of the hot water extract from willow inner bark dominated. A strong carboxylate signal at 170–180 ppm, similar to the one in the spectrum of the solid residue, was also present, possibly originating from the tannins of the outer bark. The OCH_3 signal at 58.5 ppm, characteristic of lignin, was practically absent in the precipitate in contrast to the solid residue that clearly showed the presence of OCH_3 in its solid state ^{13}C NMR spectrum (Fig. 2b). However, a weak OCH_3 peak was present in the solution state correlation spectrum of the precipitate (Fig. 4) indicating yet dissolution of some lignin from the bark. A single peak at 6.7/115 ppm appeared in the aromatic region that is typical for guaiacyl structures while no syringyl units were detected (Fig. 3). Three strong and well-resolved HSQC signals observed at 126.01/7.13, 127.81/7.20, and 129.01/7.22 ppm revealed the presence of phenylalanine in the precipitate (Fig. 3). Another peak at 129.90/7.04 ppm showed the occurrence of tyrosine. These aromatic amino acids were originally present in the bark and in the lignin preparation enzymatically isolated from it. (Dou et al., 2018b) The aliphatic carbon signals at 20–40 ppm of CP/MAS spectra of the precipitates from the bark may indicate that they contained some suberin even though not to the extent that the solid residues did (Figures S9 and S10).

In conclusion, it looks like the material precipitated from the spent liquor after the *p*-TsOH treatment was almost pure, slightly modified lignin in the case of willow wood. In contrast, the corresponding precipitate from willow bark contained hardly any lignin. Obviously, the condensation with the low molecular weight components, i.e. the aromatic extracts and hydroxymethylfurfural formed from fructose, completely prevented the delignification of willow bark. Figure S11 visualizes the aggregates of the materials precipitated from the spent aqueous *p*-TsOH by water.

3.3. Structure and properties of LCNF and LCNF films

After washing with water, the solid residues from the aqueous *p*-TsOH treatments were fibrillated with a super mass colloider (SMC). The structure of the thus formed lignin-containing cellulose nanofibrils (LCNF) was imaged by atomic force microscopy (AFM). The average fibril size, measured as the fibril height, decreased gradually from ca. 60 nm to 15 nm when the fibrillation time was increased in steps from 15 min to 60 min (Fig. 5). Increasing the concentration of *p*-TsOH from 60% to 80% facilitated faster fibrillation of the solid residue to thinner fibrils (Figure S12). Additionally, small and globular-shaped particles, obviously representing the residual lignin or the other hydrophobic substances present in the solid residues, were visible especially after fractionation with 60% *p*-TsOH. Scanning electron microscopy (SEM) images revealed fibril networks and globular-shaped particles similar to the AFM images (Fig. 6 and Figure S13). When willow bark was fractionated with 60% *p*-TsOH, fibrillation of the solid residue consumed substantially less energy than the solid residue of the wood did (Table S3). However, the difference between the bark and wood was not observed after fractionation with 80% *p*-TsOH that resulted in significantly reduced fibrillation energy demand.

The thermal stability of the original willow wood, willow bark and the LCNF made of them was studied by thermogravimetric analysis (TGA). LCNF prepared of the bark were thermally more stable than the wood derived LCNF (Fig. 7). Use of 80% *p*-TsOH in the fractionation of the wood resulted in LCNF with especially low thermal stability. In part, the thermal durability seemed to relate with the chemical composition of the LCNF. Thus, the high stability of the bark derived LCNF obviously originated from their low content of polysaccharides that are thermally less stable than lignin and its condensation products which were abundant in LCNF made of bark.

The hydrophobicity of the LCNF films (Figure S14) was evaluated through measuring the contact angle of water droplets on the films by photography. The films of bark LCNF were more hydrophobic (higher water contact angle) than the wood LCNF films (Table 3). Using 60% *p*-TsOH in the fractionation of the bark (or wood) was beneficial for hydrophobicity of the films. The highest average water contact angle measured (104°) was slightly higher than the contact angle of a resin modified CNF (θ = 101°). (Sakakibara et al., 2016) The hydrophobicity of the bark LCNF films must be related with their chemical composition, the high residual lignin content in combination with the other acid insoluble substances, such as the condensed hydroxymethylfurfural and aromatic extracts as well as suberin (Schreiber, 2010; Riley and Kolattukudy, 1975). On microscopic level the hydrophobicity could be explained by the presence of the nano-sized globular particles of the hydrophobic substances (Fig. 5).

The most hydrophobic LCNF made of willow bark demonstrated also the lowest moisture sorption at constant humidity (Fig. 8). However, the hysteresis phenomenon was more pronounced with the bark LCNF which may indicate slower equilibration of the more hydrophobic materials (Table S4 and Figure S15). Thus, fluctuations in relative humidity may significantly affect the material properties of LCNF (Table 4).

Surprisingly, the most hydrophobic LCNF produced films of the highest tensile index and breaking strain even though the elastic modulus was unaffected by the origin of LCNF (Table 4) (Rojo et al., 2015).

4. Conclusions

A promising and low-cost mean to produce strong, dense and highly hydrophobic films from otherwise discarded willow bark was developed. The bark was first treated with an aqueous *p*-TsOH hydrotrope at 80 °C for 20 min and the solid residue was then mechanically fibrillated to nano-sized structures (lignin containing nanofibrils, LCNF). Hot pressing of LCNF produced dense films with variable properties depending on the pretreatment conditions. Thus, it was possible to produce very hydrophobic LCNF films that were also strong. The films made of willow bark were highly resistant to water vapor, probably due

to the condensation of the residual lignin with the low molecular weight aromatic substances of bark and hydroxymethylfurfural formed *in situ* under the acidic fractionation conditions. Suberin of the bark seemed also to contribute on the hydrophobicity of the films.

Acknowledgments

The authors thank Tuuli Uimonen, Rita Hatakka, Ritva Kivelä and Jani Seitsonen from Aalto University for their skillful assistance in DVS, HPAEC, AFM and TEM, respectively. This work made use of the Aalto University Nanomicroscopy Center (Aalto-NMC) premises. Finally, we would like to thank Prof John Ralph for his scientific advice and for letting us use the NMR facilities from the Department of Biochemistry and The DOE Great Lakes Bioenergy Research Center, the University of Wisconsin-Madison. JR was funded by the DOE Great Lakes Bioenergy Research Center (DOE BER Office of Science DE-FC02-07ER64494). JD was funded by the three-year grant from Finnish Cultural Foundation.

Appendix A. Supplementary data

Supplementary material related to this article can be found, in the online version, at doi:https://doi.org/10.1016/j.indcrop.2018.11.033.

References

Bian, H., Chen, L., Gleisner, R., Dai, H., Zhu, J.Y., 2017. Producing wood-based nanomaterials by rapid fractionation of wood at 80 °C using a recyclable acid hydrotrope. Green Chem. 19, 3370–3379.

Chen, L., Wang, Q., Hirth, K., Baez, C., Agarwal, U.P., Zhu, J.Y., 2015. Tailoring the yield and characteristics of wood cellulose nanocrystals (CNC) using concentrated acid hydrolysis. Cellulose 22, 1753–1762.

Chen, L., Zhu, J.Y., Baez, C., Kitin, P., Elder, T., 2016. Highly thermal-stable and functional cellulose nanocrystals and nanofibrils produced using fully recyclable organic acids. Green Chem. 18, 3835–3843.

Chen, L., Dou, J., Ma, Q., Li, N., Wu, R., Bian, H., Yelle, D.J., Vuorinen, T., Fu, S., Pan, X., Zhu, J.Y., 2017. Rapid and near-complete dissolution of wood lignin at ≤80°C by a recyclable acid hydrotrope. Sci. Adv. 3, e1701735.

Dönmez, I.E., Hemming, J., Willför, S., 2016. Bark extractives and suberin monomers from *Arbutus andrachne* and *Platanus orientalis*. BioResources 11, 2809–2819.

Dou, J., Galvis, L., Holopainen-Mantila, U., Reza, M., Tamminen, T., Vuorinen, T., 2016. Morphology and overall chemical characterization of willow (*Salix* sp.) inner bark and wood: toward controlled deconstruction of willow biomass. ACS Sustain. Chem. Eng. 4, 3871–3876.

Dou, J., Xu, W., Koivisto, J.J., Mobley, J.K., Padmakshan, D., Kögler, M., Xu, C., Willför, S., Ralph, J., Vuorinen, T., 2018a. Characteristics of hot water extracts from the bark of cultivated willow (*Salix* sp.). ACS Sustain. Chem. Eng. 6 (4), 5566–5573.

Dou, J., Kim, H., Li, Y., Padmakshan, D., Yue, F., Vuorinen, T., Ralph, J., 2018b. Structural characterization of Lignins from willow bark and wood. J. Agric. Food Chem. 7294–7300.

Espinosa, S.C., Kuhnt, T., Foster, E.J., Weder, C., 2013. Isolation of thermally stable cellulose nanocrystals by phosphoric acid hydrolysis. Biomacromolecules 14, 1223–1230.

Ferreira, R., Garcia, H., Sousa, A.F., Guerreiro, M., Duarte, F.J.S., Freire, C.S.R., Calhorda, M.J., Silvestre, A.J.D., Kunz, W., Rebelo, L.P.N., Pereira, C.S., 2014. Unveiling the dual role of the cholinium hexanoate ionic liquid as solvent and catalyst in Suberin Depolymerisation. RSC Adv. 4, 2993–3002.

Frangville, C., Rutkevičius, M., Richter, A.P., Velev, O.D., Stoyanov, S.D., Paunov, V.N., 2012. Fabrication of environmentally biodegradable lignin nanoparticles. ChemPhysChem 13, 4235–4243.

Giese, M., Blusch, L.K., Khan, M.K., MacLachlan, M.J., 2015. Functional materials from cellulose-derived liquid-crystal templates. Angew. Chem. Int. Ed. 54, 2888–2910.

Graça, J., 2015. Suberin: the biopolyester at the frontier of plants. Front. Chem. 3, 1–11.

Hoeger, I.C., Nair, S.S., Ragauskas, A.J., Deng, Y., Rojas, O.J., Zhu, J.Y., 2013. Mechanical deconstruction of lignocellulose cell walls and their enzymatic saccharification. Cellulose 20, 807–818.

Idström, A., Schantz, S., Sundberg, J., Chmelka, B.F., Gatenholm, P., Nordstierna, L., 2016. ^{13}C NMR assignments of regenerated cellulose from solid-state 2D NMR spectroscopy. Carbohydr. Polym. 151, 480–487.

Kim, H., Ralph, J., 2010. Solution-state 2D NMR of ball-milled plant cell wall gels in DMSO-*d*6/Pyridine-*d*5. Org. Biomol. Chem. 8, 576–591.

Kim, H., Ralph, J., Akiyama, T., 2008. Solution-state 2D NMR of ball-milled plant cell wall gels in DMSO-d6. BioEnergy Res. 1, 56–66.

Kim, H., Padmakshan, D., Li, Y., Rencoret, J., Hatfield, R.D., Ralph, J., 2017. Characterization and elimination of undesirable protein residues in plant cell wall materials for enhancing lignin analysis by solution-state nuclear magnetic resonance spectroscopy. Biomacromolecules 18, 4184–4195.

Kono, H., Yunoki, S., Shikano, T., Fujiwara, M., Erata, T., Takai, M., 2002. CP/MAS ^{13}C NMR study of cellulose and cellulose derivatives. 1. Complete assignment of the CP/MAS ^{13}C NMR spectrum of the native cellulose. J. Am. Chem. Soc. 124, 7506–7511.

Krzyżaniak, M., Stolarski, M.J., Szczukowski, S., Tworkowski, J., Bieniek, A., Mleczek, M., 2015. Willow biomass obtained from different soils as a feedstock for energy. Ind. Crops Prod. 75, 114–121.

Ma, Y., Asaadi, S., Johansson, L.-S., Ahvenainen, P., Reza, M., Alekhina, M., Rautkari, L., Michud, A., Hauru, L., Hummel, M., Sixta, H., 2015. High-strength composites fibers from cellulose-lignin blends regenerated from ionic liquid solution. ChemSusChem 8, 4030–4039.

Österberg, M., Vartiainen, J., Lucenius, J., Hippi, U., Seppälä, J., Serimaa, R., Laine, J., 2013. A fast method to produce strong NFC films as a platform for barrier and functional materials. ACS Appl. Mater. Interfaces 5, 4640–4647.

Pääkkönen, T., Dimic-Misic, K., Orelma, H., Pönni, R., Vuorinen, T., Maloney, T., 2016. Effect of xylan in hardwood pulp on the reaction rate of TEMPO-mediated oxidation and the rheology of the final nanofibrillated cellulose gel. Cellulose 23, 277–293.

Perra, B., Haluk, J.-P., Metche, M., 1993. Extraction of Suberin and lignin from Beech Barks (*Fagus sylvatica* L.). Holzforschung 47, 486–490.

Qin, Y., Qiu, X., Zhu, J.Y., 2016. Understanding longitudinal wood Fiber ultra-structure for producing cellulose nanofibrils using disk milling with diluted acid prehydrolysis. Sci. Rep. 6, 35602.

Rajala, S., Siponkoski, T., Sarlin, E., Mettänen, M., Vuoriluoto, M., Pammo, A., Juuti, J., Rojas, O.J., Franssila, S., Tuukkanen, S., 2016. Cellulose nanofibril film as a piezoelectric sensor material. ACS Appl. Mater. Interfaces 8, 15607–15614.

Riley, R.G., Kolattukudy, P.E., 1975. Evidence for covalenty attached *p*-Coumaric acid and ferulic acid in Cutins and suberins. Plant Physiol. 56, 650–654.

Rojo, E., Peresin, M.S., Sampson, W.W., Hoeger, I.C., Vartiainen, J., Laine, J., Rojas, O.J., 2015. Comprehensive elucidation of the effect of residual lignin on the physical, barrier, mechanical and surface properties of nanocellulose films. Green Chem. 17, 1853–1866.

Saito, T., Isogai, A., 2004. TEMPO-mediated oxidation of native cellulose. The effect of oxidation conditions on chemical and crystal structures of the water-insoluble fractions. Biomacromolecules 5, 1983–1989.

Sakakibara, K., Yano, H., Tsujii, Y., 2016. Surface engineering of cellulose nanofiber by adsorption of diblock copolymer dispersant for green nanocomposite materials. ACS Appl. Mater. Interfaces 8, 24893–24900.

Sannigrahi, P., Kim, D.H., Jung, S., Ragauskas, A., 2011. Pseudo-lignin and pretreatment chemistry. Energy Environ. Sci. 4, 1306–1310.

Schreiber, L., 2010. Transport barriers made of cutin, suberin and associated waxes. Trends Plant Sci. 15, 546–553.

Trockenbrodt, M., 1994. Light and Electron Microscopic investigations on wound reactions in the bark of *Salix caprea* L. and *Tilia tomentosa* moench. Flora 189, 131–140.

van Zandvoort, I., Wang, Y., Rasrendra, C.B., van Eck, E.R.H., Bruijnincx, P.C.A., Heeres, H.J., Weckhuysen, B.M., 2013. Formation, molecular structure, and morphology of humins in biomass conversion: influence of feedstock and processing conditions. ChemSusChem 6, 1745–1758.

Wang, R., Chen, L., Zhu, J.Y., Yang, R., 2017. Tailored and integrated production of carboxylated cellulose nanocrystals (CNC) with nanofibrils (CNF) through maleic acid hydrolysis. ChemNanoMat 3, 328–335.

Yelle, D.J., Ralph, J., Frihart, C.R., 2008. Characterization of nonderivatized plant cell walls using high-resolution solution-state NMR spectroscopy. Magn. Reson. Chem. 46, 508–517.

Zhu, H., Luo, W., Ciesielski, P.N., Fang, Z., Zhu, J.Y., Henriksson, G., Himmel, M.E., Hu, L., 2016. Wood-derived materials for green electronics, biological devices, and energy applications. Chem. Rev. 116, 9305–9374.